Marine Geology
June 2009, Volume 261, Issues 1-4, Pages 114-127
http://dx.doi.org/10.1016/j.margeo.2009.02.001

Microbial methane oxidation and sulfate reduction at cold seeps of the deep Eastern Mediterranean Sea

Enoma O. Omoregie[a, b, 1, *], Helge Niemann[a, 2], Vincent Mastalerz[c], Gert J. de Lange[c], Alina Stadnitskaia[d], Jean Mascle[e], Jean-Paul Foucher[f] and Antje Boetius[a, b, g, *]

[a] Max Planck Institute for Marine Microbiology, Bremen, Germany
[b] Jacobs University Bremen, Bremen, Germany
[c] Department of Earth Sciences, Utrecht University, Utrecht, The Netherlands
[d] Royal Netherlands Institute for Sea Research (NIOZ), Texel, The Netherlands
[e] Geosciences-Azur, Villefranche sur mer, France
[f] Department of Marine Geosciences, IFREMER Centre de Brest, Plouzane Cedex, France
[g] Alfred Wegener Institute for Polar and Marine Research, Bremerhaven, Germany
[1] Present address: School of Earth, Atmospheric and Environmental Sciences, The University of Manchester, Oxford Road, Manchester M13 9PL, UK. Tel.: +44 161 275 5668; fax: +44 161 306 9361.
[2] Present address: Institute for Environmental Geosciences, University of Basel, Basel, Switzerland.

*: Corresponding author : Enoma O. Omoregie, Tel.: +49 421 2028 860; fax: +49 421 2028 690, email address : enoma.omoregie@manchester.ac.uk, Antje Boetius, email address : aboetius@mpi-bremen.de

Abstract:

The Eastern Mediterranean hosts a variety of active cold seep systems, such as gas chimneys, mud volcanoes and pockmarks, in water depths of 500 to 3200 m. As part of the NAUTINIL expedition in 2003, the sediments of cold seeps on the Nile Deep Sea Fan (NDSF) were sampled for the first time for biogeochemical and microbiological analyses. Here we compare rates of the anaerobic oxidation of methane (AOM) and sulfate reduction (SR) as well as the microbial community structure of a variety of cold seep systems including mud volcanoes, pockmarks and brine seeps. Our results revealed strong differences in microbial activity among the different seep systems of the Eastern, Central and Western provinces of the NDSF, as well as the Olimpi field (Central Mediterranean Ridge). Integrated over a sediment depth of 10 cm below the seafloor, SR rates ranged from 0.1–66 mmol m^{-2} d^{-1} and AOM rates from 0.1–3.6 mmol m^{-2} d^{-1}. SR was often considerably higher than methane oxidation, indicating that electron donors other than methane were utilized. In general, the lowest rates were associated with pockmarks and carbonate pavements, and highest rates with bacterial mats above the gassy sediments of mud volcano centers. 16S rRNA gene analysis and fluorescence in situ hybridization (FISH), revealed the presence of all known groups of marine methane oxidizing *Archaea* (i.e. ANME-1, -2, -3) and also of methane oxidizing *Bacteria* (i.e. *Methylobacter* sp. and relatives) in some seep sediments. Presumably syntrophic sulfate-reducing bacterial partners of ANMEs were also detected in association with the ANMEs. Several ANMEs formed consortia with unknown bacterial partners. The microbial community structure reflected the presence of typical seep microorganisms at all sites investigated, but differed to varying extents between the different types of seeps. Despite the high availability of methane and sulfate, methanotrophic microbial activity and biomass were lower at the seeps of the Eastern Mediterranean compared to those of other continental margins for unknown reasons.

Keywords: methane oxidation; sulfate reduction; *Archaea*; cold seeps; mud volcano; pockmarks; Nile Deep Sea Fan

1. Introduction

Cold seeps are geologically and geochemically active seafloor systems that often host dense and diverse microbial and faunal communities fueled by fluid and gas emissions to the sea floor (Sibuet and Olu, 1998; Treude et al., 2003; Levin, 2005; Niemann et al., 2006a; Niemann et al., 2006b; Omoregie et al., 2008). A variety of such cold seep systems, including mud volcanoes, pockmarks and brine lakes, have recently been detected on the active ridges and passive continental margins of the Eastern Mediterranean. Accumulations of fluid escape structures are found at the Eastern Mediterranean ridge accretionary prism (Camerlenghi et al., 1992; Fusi and Kenyon, 1996; Woodside et al., 1998; Huguen et al., 2004; Huguen et al., 2005; Zitter et al., 2005), the Nile Deep Sea Fan (NDSF) off the coast of Egypt (Mascle et al., 2001; Loncke et al., 2004; Loncke et al., 2006; Dupré et al., 2007) and off the coast of Israel (Coleman and Ballard, 2001). Due to the importance of methane as a greenhouse gas, increasing attention has been given to the structure, function and distribution of cold seep communities, which may act as a biological barrier to methane emission ((Hinrichs and Boetius, 2002; Sibuet and Olu-Le Roy, 2002; Reeburgh, 2007) and references therein).

One of the main biogeochemical processes underlying energy flow in cold seep ecosystems is the anaerobic oxidation of methane (AOM) via sulfate reduction (SR) (Boetius et al., 2000a; Michaelis et al., 2002; Treude et al., 2003; Niemann et al., 2006b). This process significantly affects seep habitats by inducing the precipitation of carbonate (Ritger et al., 1987; Wallmann et al., 1997) and by producing sulfide, both of which provide additional niches to a variety of microbial communities and benthic fauna, including chemosynthetic microbe-animal symbioses, such as in siboglinid tubeworms,

mytilids and vesicomyid bivalves (Sibuet and Olu-Le Roy, 2002). AOM is mediated by a presumably syntrophic association between *Methanosarcinales*, *Methanomicrobiales* and *Methanococcoides* related anaerobic methanotrophic archaea (ANME groups 1-3) and sulfate-reducing b*acteria* (SRB) of the *Desulfosarcina*/*Desulfococcus* or the *Desulfobulbus* clusters (Boetius et al., 2000a; Orphan et al., 2001; Knittel et al., 2005; Niemann et al., 2006b; Lösekann et al., 2007). A distinct variety of other bacteria and archaea have been repeatedly detected associated with ANME in cold seep systems, however, their function remains unknown (Knittel et al., 2003; Knittel et al., 2005; Mills et al., 2005).

The Eastern Mediterranean basin is known as one of the most oligotrophic areas of the world's oceans. It is characterized by low particle flux rates, deep oxygen and sulfate penetration into the seafloor, due to low rates of organic matter mineralization and low microbial cell numbers (Boetius and Lochte, 1996). Hence, sulfidic environments at the deep seafloor of the Eastern Mediterranean are typically associated with local advection of electron donors from the deep subsurface, such as by fluid flow and gas seepage. Active cold seep systems in the Eastern Mediterranean have been the subject of several studies that have included mud volcanoes on the Eastern Mediterranean Ridge, such as Napoli and Milano in the Olimipi area and Amsterdam and Kazan in the Anaximander mountains (Aloisi et al., 2000; Pancost et al., 2000; Aloisi et al., 2002; Charlou et al., 2003; Haese et al., 2003; Heijs, 2005; Mills et al., 2005; Bouloubassi et al., 2006; Heijs et al., 2006). Highly ^{13}C-depleted archaeal biomarkers (i.e. archaeol, 2,6,10,15,19-pentamethylicosane (PMI) and others), indicative of AOM, have been recovered from carbonates and sediments at these seeps (Aloisi et al., 2000; Pancost et al.,

2000; Aloisi et al., 2002; Heijs, 2005; Bouloubassi et al., 2006; Heijs et al., 2006). Evidence for SR coupled to AOM at these sites has been made primarily on the basis of ^{13}C-depleted bacterial lipids, believed to originate from methane dependent SRB (Aloisi et al., 2000; Pancost et al., 2000; Aloisi et al., 2002; Heijs, 2005; Bouloubassi et al., 2006; Heijs et al., 2006). Furthermore, 16S rRNA gene surveys of sediments from these mud volcanoes have revealed the presence of different types of ANME (Heijs, 2005; Heijs et al., 2005), i.e. ANME-1 and 2, as well as their sulfate reducing partners, which are related to the *Desulfosarcina*/*Desulfococcus cluster*.

Here we present the first AOM and SR activity measurements, in relation to microbial community structure, of cold seep systems of the NDSF. We focused on cold seeps of the Eastern (Amon, Isis mud volcanoes), Central (North Alex mud volcano, pockmark areas) and Western (Chefren mud volcano) NDSF, as well as on the Napoli mud volcano of the Olimpi field on the Central Mediterranean Ridge. We used whole core tracer injection methods to quantify rates of methane oxidation and sulfate reduction, and 16S rDNA-based molecular tools to investigate the microbial community structure. The questions addressed by this study were: (1) What is the range of microbial methane and sulfate consumption at different types of seeps of the NDSF? (2) Which key microorganisms mediate these processes?

2. Regional settings

A detailed description of the geology and evolution of fluid escape structures on the NDSF has been published recently (Mascle et al., 2006; Dupré et al., 2007) and is

122 provided in this volume by Huguen et al., (Huguen et al., In review, this volume). Fluid
123 escape structures and associated mud volcanoes are abundant on the Mediterranean Ridge
124 accretionary prism (Fusi and Kenyon, 1996; Huguen et al., 2004), and on the
125 Anaximander Mountains between the Hellenic and Cyprus arcs (Woodside et al., 1998;
126 Zitter et al., 2005). More recently, seepage activity was discovered on the NDSF
127 ((Loncke et al., 2004; Mascle et al., 2005; Mascle et al., 2006) and references therein).
128 Most of the NDSF was formed in the late Miocene and corresponds at present to the most
129 prominent sedimentary structure of the Eastern Mediterranean margin, with thick
130 sediment deposits of more than 9–10km. The fluid escape structures of the Eastern,
131 Central and Western province of the NDSF investigated here appear connected to salt
132 tectonics and subsequent gravitational forces causing a spreading and gliding of the thick
133 sedimentary packages on the NDSF. Furthermore, the Egyptian slope is a prolific domain
134 for hydrocarbons with its large subsurface gas and oil reservoirs (Dolson et al., 2002);
135 and these fuel many active fluid escape structures on the NDSF of which only few have
136 been investigated to date.
137 The mud volcanoes Amon and Isis of the Eastern NDSF, North Alex of the
138 Central NDSF (Dupré et al., 2007); and Chefren and Mykerinos of the Western NDSF
139 (Huguen et al., In review, this volume), were sampled for the first time with the
140 submersible Nautile (IFREMER) during the NAUTINIL expedition in 2003 (Fig. 1).
141 These mud volcanoes are circular features (1-3 km in diameter) in water depths of 500 -
142 3000 m with elevations of up to 100 m above the seabed (Dupré et al., 2007). They are
143 located above well-developed feeder channels, clearly seen in the seismic data (Loncke et
144 al., 2004; Dupré et al., 2007; Huguen et al., In review, this volume). In the deeper central

province of the NDSF we sampled a field characterized by abundant pockmarks of 3-15 m diameter between extensive flat carbonate pavements covering the seafloor (Bayon et al., In review, this volume). For comparison, we also investigated a fluid escape structure on the central Mediterranean Ridge, the Napoli mud volcano, which is located within the Olimpi area (Camerlenghi et al., 1992; Huguen et al., 2005) (Fig. 1).

3. Material and Methods

At all sites, sediment samples were collected by blade (Width × Height × Length:10×25×40 cm) and push corers(Diameter × Length: 5×25 cm) by the submersible *Nautile*. Generally, cores were retrieved on board less than 5 hours after coring. Immediately upon returning to the RV *L'Atalante*, the cores were taken to the cold room, sub-sampled and processed for the measurements outlined below. Table 1 list the cores recovered from each site as well as their treatment.

3.1 Methane concentration

Due to sampling constraints, methane concentration data from two different types of initial processing methods were included within this study. The sediments were sectioned horizontally (2 cm intervals, corresponding to 2 ml of sediment) and placed in 18 ml glass vials containing 10 ml of 2.5% NaOH. The vials were immediately sealed with rubber stoppers. Alternatively, sections were equilibrated with a saturated NaCl solution (ca. 300 g/l) in rubber sealed glass vials for at least 12 hours. The sediment slurries were shaken, and 100 µl of headspace removed by a glass syringe. Methane

concentrations were measured by injecting 100 µl of headspace in a Hewlett Packard 5890A or a Shimadzu GC-14B gas chromatograph. The detector for both chromatographs was a flame ionization detector.

3.2 *Methane oxidation*

Methane oxidation rates were measured using dissolved $^{14}CH_4$, based on previously described methods (Iversen and Blackburn, 1981; Treude et al., 2003). Pre-drilled cores were used to sub-sample the push cores. The holes were spaced 1 cm apart and sealed with silicone prior to sub-sampling. Immediately after sub-sampling, subcores were sealed with a rubber stopper and placed in the dark at the *in situ* temperature of 14°C for 1 - 2 hours. Ten microliters of $^{14}CH_4$ (~0.25 kBq) were then injected through the silicon plugs into the sediment, and the sub-cores were incubated in the dark at *in situ* temperature for 24 hr. The cores were then quickly sectioned into 2 cm layers, and the sections fixed in 10 ml of 2.5% NaOH as for methane concentration determinations. Further processing was done according to Treude et al. (Treude et al., 2003). Rates were calculated according to the equation below, where $^{14}CO_2$ = activity of CO_2 produced, $^{14}CH_4$= activity of residual tracer, CH_4 = residual CH_4, *V*= sediment volume and *t*= incubation time.

$$\text{AOM rate} = (^{14}CO_2/(^{14}CO_2 + {}^{14}CH_4)) \times [CH_4] / V / t$$

3.3 Sulfate concentration

As with methane concentration measurements, two separate methods were used to initially process and measure sulfate concentrations. Subcores were sectioned

191 horizontally (2 cm intervals, corresponding to 2 ml of sediment) and sections were placed
192 in 15 ml polypropylene vials with 5 ml of 20 % zinc acetate and shaken thoroughly. The
193 sediment slurry was then centrifuged at 5000 rpm for five minutes and the supernatants
194 removed and transferred to clean polypropylene vials. The supernatants were analyzed
195 using non-suppressed ion chromatography with an anion exchange column (LCA A14,
196 Sykam) and a conductivity detector (S3110, Sykam). Alternatively, pore water was
197 squeezed from the sediment sections and sulfate measured as S using inductively coupled
198 plasma atomic emission spectroscopy (ICP-AES).
199
200 *3.4. Sulfate reduction*
201 Sulfate reduction rates were measured by $^{35}SO_4^{-2}$ whole core injection incubations
202 (Treude et al., 2003). Parallel to the methane oxidation samples, sediment subcores were
203 pre-incubated, injected with 5 µl of $^{35}SO_4^{-2}$ (10 kBq) and incubated for 24 hours at *in situ*
204 temperature before fixation in 5 ml of 20% zinc acetate. The samples were then
205 processed according the method described by Kallmeyer et al. (Kallmeyer et al., 2004).
206 Rates were calculated according to the equation below, where $TRI^{35}S$ = activity of total
207 reduced inorganic sulfur, $^{35}SO4$ = activity of residual tracer, SO_4^{-2} = residual SO_4^{-2}
208 within the sample, V = sediment volume, and t = time.

209 $$SR\ rate = (TRI^{35}S/(TRI^{35}S + {}^{35}SO_4^{-2})) \times [SO_4^{-2}]\ /\ V\ /\ t$$

210
211 *3.5 Acridine Orange Direct Counts (AODC) and Fluorescence In Situ Hybridization*
212 *(FISH)*
213 Two milliliters of sediment were placed in a 20 ml plastic tube with 9 ml of a 2 %
214 formalin and artificial seawater solution for 4 hr at room temperature. At the end of the

incubation period, half of the mixture was washed twice in PBS and stored in a PBS\ethanol solution (50:50) at -20°C for FISH, the other half was stored at 4°C for AODC. AODC (Boetius and Lochte, 1996), FISH (Snaidr et al., 1997) and CARD-FISH (Pernthaler et al., 2002; Ishii et al., 2004) were all performed according to previously described methods. All FISH and CARD-FISH slides were counter-stained with DAPI (4´,6´- diamidino-2-phenylindole). At least 30 - 50 grids were counted randomly from each slide for AODC, FISH and CARD-FISH. Probe hybridization details are given in Table 2. No signal was observed using the ANME-2, and Mγ705 CARD-FISH probes, therefore ANME-2 and Mγ705 targeted cells were enumerated using monolabeled FISH probes. Cell numbers within conspicuous ANME-SRB aggregates were estimated using a semi-direct method (Boetius et al., 2000b). All aggregates and cells were assumed to be spherical. The average cell volume was estimated to be 0.065 μm^3. The volume of an average aggregate (82 μm^3) was determined by randomly measuring the diameter of 50 aggregates on filters from Amon (NL12PC2) and Chefren (NL18PC2(7)). The average aggregate volume was divided by the average cell volume, and a ratio of 1:1 archaeal to bacterial cells was used to calculate the number of bacterial and archaeal cells per aggregate.

3.6 16S rDNA library construction and analysis

Sediments were sectioned into 2 cm intervals and frozen at -20°C until further processing. 16S rDNA libraries for Archaea and B*acteria* were created after Niemann et al. (Niemann et al., 2006a). Briefly, total DNA was extracted from the first 4 cm of sediment (~ 0.3 g) with the FastDNA spin kit for soil, essentially following the

manufacture's recommendations (Q-Biogene, Irvine, California, USA). Partial 16S genes were amplified using the primers ARCH20F (Massana et al., 1997) and Uni1392R (Lane et al., 1985) for *Archaea* and GM3F (Muyzer et al., 1995) and GM4R (Kane et al., 1993) for *Bacteria*. Amplification products were then cloned and sequenced in one direction on an ABI 3100 genetic analyzer. Single directional reads were then added to preexisting phylogenetic trees using the parsimony tool in the ARB software package (Ludwig et al., 2004) to determine their phylogenetic affiliations. P-tests were conducted for comparisons between sequence libraries in this study using the program S-LIBSHUFF version 1.22 (Schloss et al., 2004). Distance matrices were created in ARB (Ludwig et al., 2004) using the Neighbor-joining tool. Sequences were submitted to the GenBank database (http://www.ncbi.nlm.nih.gov/) and are accessible under the following accession numbers: EF687258-EF687340, EF687432-EF687519, EF687520-EF687656 and EU178928-EU179209

4 Results and Discussion

Previous to this investigation, the activity at cold seeps within the NDSF with regard to fluid escape, hydrocarbon oxidation, sulfide production and the composition of seep-associated benthic microbial communities was unknown. A variety of fluid escape structures, including mud volcanoes, brine seeps and pockmarks were visited in September 2003 by the expedition NAUTINIL. Most strikingly, almost all structures showed signs of active gas seepage, fluid flow, mud volcanism and authigenic carbonate formation (Dupré et al., 2007; Bayon et al., In review, this volume; Huguen et al., In review, this volume). Hence, the abundances of cold seeps, sites of hydrocarbon

emission, chemosynthetic communities and anoxic microbial ecosystems in the highly oligotrophic Eastern Mediterranean are much greater than previously considered.

4.1 Eastern province of the NDSF

4.1.1 Dive observations

Five dives were dedicated to investigating the methane turnover and microbiology of active sites of the Amon and Isis mud volcanoes (Figs. 1A,B and Table 1). For detailed geological and morphological descriptions of Amon and Isis see Dupre et al. (Dupré et al., 2007; Bayon et al., Submitted). Visual observations of both mud volcanoes provided evidence for active seepage and methane consumption at their centers. We observed areas of highly disturbed seafloor, with fresh cracks, troughs and grayish mud breccia. Blackish, reduced sediment patches of 0.5 - 4 m in diameter were also observed around the freshly disturbed areas. These were frequently covered with mats of sulfide-oxidizing b*acteria* (Fig. 2A,B). Our sampling efforts concentrated on those sites, as the presence of sulfide-oxidizing bacterial mats point to active subsurface processes producing and transporting sulfide to the seafloor (Treude et al., 2003; Niemann et al., 2006b; Bayon et al., In review, this volume).

Two sediment push cores were recovered from black sediment patches in the center of Amon (Table 1, Fig. 2A: NL11PC1, NL12PC2) and three pushcores from such microhabitats in the center of Isis (Table 1, Fig. 2B: NL8PC1(4), NL18PC3(1) and NL13PC4(7)). Sporadic gas ebullition from the seafloor was observed at Amon and Isis upon sampling and submersible touch-down in the center of these mud volcanoes. The

284 sedimentology of all push cores from the active centers of both mud volcanoes was
285 consistent with our visual observations in pointing towards active mud volcanism and
286 advective transport of hydrocarbons (Fig. 3A,B). The surfaces of both cores from Amon
287 were covered with sulfide-oxidizing bacterial mats above reduced sediments followed by
288 lighter grayish mud breccia below (Fig. 3a). All three cores recovered from Isis (Fig. 3B)
289 contained dark grey mud breccia and two cores had small whitish aggregates at the
290 surface indicating the presence of sulfide-oxidizing bacteria (NL8PC1(4), NL8PC3(1)).
291 The local variation in terms of topography and sedimentology at both mud volcanoes is
292 not surprising, given that fluid and gas flow at most cold seeps is focused, which can
293 result in large sediment heterogeneities (Sahling et al., 2002; Luff and Wallmann, 2003).
294
295 *4.1.2 Sulfate reduction and anaerobic oxidation of methane*
296 Large gas plumes with high concentrations of methane have been detected above
297 the centers of Amon and Isis (0.5 and 0.7 µM, respectively), indicating recent gas
298 ebullition at both mud volcanoes (Dupré et al., 2007). When retrieved to deck, all cores
299 from the center of Isis and Amon had cracks within the sediment indicating gas escape
300 during recovery. Accordingly, methane concentrations measured in all recovered
301 sediment cores from both mud volcanoes centers exceeded 1 mM (Fig. 3A,B), and some
302 cores still contained gas bubbles during sub-sampling. Despite high methane
303 concentrations, sulfate concentrations exceeded 5 mM throughout the cores, with
304 moderate anaerobic oxidation of methane (AOM) rates (0.1 - 3.7 mmoles x m^{-2} x d^{-1}).
305 Sulfate reduction (SR) rates (0.7 - 24 mmoles x m^{-2} x d^{-1}) were much higher (Table 3).
306 The peaks in SR coincided with reduced sediment layers stained black by FeS

307 precipitation in the cores from Amon (Fig. 3A) and one from Isis (NL8PC1(4)). In two
308 cores from Isis (NL8PC3(1)) and (NL13PC4(7)), SR activity was distributed evenly
309 throughout the cores but blackish sediment layers were not observed. SR activity
310 exceeded that of AOM by several fold and may have been supported by other electron
311 donors, transported together with methane. C_2 and higher hydrocarbons have been
312 detected in sediments and bottom waters of Amon and Isis (Dupré et al., 2007). A
313 decoupling of AOM and SR in the presence of higher hydrocarbons has already been
314 observed in seep sediments of the Gulf of Mexico (Joye et al., 2004) and the Gulf of
315 Cadiz (Niemann et al., 2006a). Sulfate reducers are capable of using a wide variety of
316 hydrocarbons as electron donors; hence it is likely that the availability of higher
317 hydrocarbons selects for other sulfate reducers besides the ANME partner SRB, as the
318 energy yield from AOM is very low (Widdel and Rabus, 2001; Widdel et al., 2006/2007;
319 Kniemeyer et al., 2007).
320
321 *4.1.3 Microbial community structure*
322 Total cell numbers were 10^8-10^9 cells x ml^{-1} in surface sediments of both mud
323 volcanoes (Table 4), which is the lower end of numbers observed at other active seep
324 settings (>10^{10} cells x ml^{-1}) (Michaelis et al., 2002; Knittel et al., 2003; Tina Lösekann et
325 al., 2007). Fluorescence in situ hybridization (FISH) (Tables 4) and 16S rRNA gene
326 analysis (Table 5) were carried out on two selected cores from Amon (NL12PC1) and Isis
327 (NL13PC4(7)), both covered by bacterial mats. These cores were selected on the basis of
328 rates, methane and sulfate concentrations, and visual characteristics indicating seepage
329 related microbial activity. The dominance (36 - 58 %) of *Deltaproteobacteria* sequences

330 in the 16S rRNA gene library for *Bacteria* of both mud volcanoes were in accordance
331 with the relatively high, near surface SR rates. A large portion of the 16S rDNA
332 sequences were related to SRB of the genera *Desulfosarcina*, *Desulfococcus*,
333 *Desulfocapsa* and *Desulfobulbus*, which are ubiquitous at seeps and have been previously
334 implicated as partners of methanotrophic archaea (ANME) (Knittel et al., 2003). The
335 probe DSS658, which targets the *Desulfosarcina/Desulfococcus* cluster, showed that
336 most of these cells were aggregated with ANME-2 cells at Amon, whereas at Isis most of
337 the DSS658 targeted cells were single cells. Compared to their high percentage in the
338 bacterial 16S rRNA gene library (19%; Tab. 4), DSS658 targeted cells made up only 2-
339 3% of the overall cell numbers at Isis, but up to 50% at Amon. Interestingly, the core
340 NL12PC1 from Amon also showed considerably closer coupling of AOM to SR. The
341 dominance of the *Archaea* libraries by sequences most closely related to ANME-2, and
342 their relatively high cell numbers was matched by relatively high AOM rates. ANME-1
343 and -3 cells were also detected, but their numbers were below 1% of the total cells.
344 Several sequences belonging to methanogens of the genus *Methanococcoides* were
345 detected in sediments of both mud volcanoes. Incubations with these sediments under
346 methanogenic conditions with methanol produced substantial enrichments of
347 *Methanococcoides* (T. Holler, unpublished data), indicating that these organisms were
348 viable. These archaea are capable of growing on C-1 compounds and could contribute to
349 local methane concentrations, however, their source of energy in the investigated
350 sediments remains unknown. Also several other typical groups of cold-seep associated
351 *Archaea* and *Bacteria* were detected (e.g. Marine Benthic Group 1(MBG1), Benthic
352 Group D (MBGD), and members of the *Gammaproteobacteria*); but the metabolic

function and environmental role of these organisms was not further investigated here. Interestingly, at both mud volcanoes a significant portion of the *Bacteria* (EUB) cells in consortium with ANME cells were not targeted by DSS658 or 660, indicating that other b*acterial* partners were present and potentially involved in AOM. This was previously also observed at other sites such as the Eel River Basin (Pernthaler et al., 2008).

Statistical tests (P value < 5%) indicated that the 16S rRNA gene library of *Archaea* at Amon was different from that at Isis. However, the reciprocal comparison (Isis to Amon) indicated no statistical difference (P value > 5%) between them, suggesting that both environments shared a subset of *Archaea*. This was also true for comparisons of the *16S rRNA gene* libraries of *Bacteria*, which indicated that the communities at both mud volcanoes were not significantly different from one another. The similarities between the microbial communities of both mud volcanoes are not surprising given their very similar geochemistry.

4.2 Central province of the NDSF

4.2.1 Dive observations

Three dives were dedicated to investigating different seafloor structures of the central province (Fig.1A, C): The active center of the North Alex mud volcano, and a region characterized by pockmarks and vast areas of carbonate crusts. For detailed morphological and geological descriptions of North Alex and the pockmarks see Dupre et al. (Dupré et al., 2007) and Bayon et al. (Bayon et al., In review, this volume). The central NDSF is comprised of three domains: an upper, middle and lower slope. The

upper slope hosts large gas chimneys associated with mud volcanoes such as North Alex. The seafloor of the center of North Alex was much less disturbed than that of Amon and Isis, and was essentially flat. However, the center sediments were overpressurized with gas, as evidenced from spontaneous gas ebullition observed during the dive (Fig. 4A). The single blade core recovered from the center was gas saturated and contained mud breccia interspersed with small chunks of carbonate (Figure 5A). Bacterial mats were not observed in the center of North Alex.

The middle slope area was characterized by a flat seafloor covered by vast areas of carbonate pavement (> 1 km) associated with empty shells and tubes, and relatively sparse patches of living chemosynthetic fauna, interspersed by reduced, grayish sediments, as well as many pockmarks (Fig. 4B). The pockmarks were circular depressions of approximately 3-15 m in diameter and up to 3 m depth below the surrounding seafloor. Carbonate crusts and chemosynthetic fauna (Fig. 4B) were observed in the central depressions of the pockmarks, indicating a connection between gas flow, microbial methane oxidation and carbonate precipitation (Bayon et al., In review, this volume). One core was taken within a small pockmark (NL6PC1), and another one (NL7PC1) from pelagic sediments of light brown color just outside of a carbonate-covered area.

The area on the lower slope also showed extensive (~ 500 m) flat and partially broken carbonate crusts, which hosted seep-associated fauna and lots of shell debris. The larger carbonate pavements on the middle and lower slope were interspersed by reduced blackish sediments (Fig. 4C), littered by shell debris. They hosted a variety of small chemosynthetic bivalves as well as small patches of living siboglinid tube worms (Fig.

399 4D). These organisms likely depended on the sulfide flux derived from hydrocarbon-
400 fueled sulfate reduction in sediments below the crust. Outside the flat area, many small
401 carbonate mounds and small (<3 m) pockmarks were observed. Here, one core was taken
402 close to a small carbonate mound (NL14PC2). In contrast to Amon, Isis and North Alex,
403 the pockmarks appeared to be an area of reduced but probably long-term seepage activity
404 as discussed by Bayon et al. (Bayon et al., In review, this volume).
405
406 *4.2.2 Sulfate reduction and anaerobic oxidation of methane*
407 Methane concentrations of up to 0.2 µM in the bottom water above the centre of
408 North Alex indicated that this mud volcano actively emitted methane, similar to Amon
409 and Isis (Dupré et al., 2007). According to the visual observations, the sediments were
410 gas-saturated at the seafloor. Methane concentrations in retrieved cores from North Alex
411 were up to 1.8 mM. In contrast, the bottom waters of the middle and lower slope areas
412 next to the pockmarks and carbonate pavements showed no or very low methane
413 anomalies (Bayon et al., In review, this volume). Correspondingly, sediment cores from
414 these areas contained less than 10 µM methane.
415 SR and AOM rates measured (Fig. 5A and Table 3) at North Alex were 4 and 3.4
416 mmol x m^{-2} x d^{-1} within the top 10 cm, respectively, indicating a tight coupling (~ 1.2:1)
417 between SR and AOM. Sulfate and methane were not completely depleted within this
418 zone, indicating that neither electron donor nor acceptor was limiting the ANME
419 community, and that advective transport methane from below was probably high. In
420 contrast, SR and AOM rates were generally < 0.1 mmol m^{-2} d^{-1} (integrated over the first
421 10 cm) at the middle slope in samples taken next to a carbonate mound within a

pockmark, as well as outside the pockmark and carbonate areas. Only the core from dive NL14 taken next to the carbonate mound (lower slope) showed higher rates (2.8 mmol x m^{-2} x d^{-1}). However, here, maximum rates were found below 10 cm sediment depth. This is consistent with observations made by Bayon et al. (Bayon et al., In review, this volume), which suggested that the sediments beneath the crusts are active in methane turnover.

4.2.3 Microbial community structure

We chose the most active samples for analysis of the distribution of different microbial groups; the core from the center of North Alex (NL15BC1) and the core next to a small carbonate mound on the lower slope (NL14PC2). Cell numbers at North Alex were $>10^9 \times$ cells $\times$ ml^{-1} in the surface sediments, but only a few consortia were detected (Table 4). Interestingly, ANME-1 and -2 cells comprised only a small part of the archaeal cells that were detected in both sediments. Furthermore, bacterial cells within the aggregates were not targeted by DSS658, indicating that unknown bacterial partners were involved in the AOM consortia. The vast majority of cells in the sediments were unknown single cell *Bacteria*; only 6 % of these were targeted by DSS658. The cell numbers from the pockmark region (NL14(PC2)) were considerably lower ($0.4 - 0.9\ 10^9$ $\times$ cells $\times$ ml^{-1}) and methane-oxidizing archaea were virtually absent from these sediments. However, microbial biomarker analysis of carbonates from this site indicated that ANME-2 were the dominant group within the carbonates (Gontharet, unpublished data, Stadnitskaia unpublished data), which suggests that AOM was of greater importance in

444 the past. Unfortunately, the active sediments below these carbonates could not be
445 sampled.
446
447 **3.3 Brine-influenced gas seeps: Western Province of the NDSF and the Olimpi mud**
448 **volcano field**
449
450 *3.3.1 Dive observations*
451 Three dives were dedicated to investigating sites of hydrocarbon and brine
452 seepage in the Western Province of the NSDF and the Olimpi field of the Central
453 Mediterranean Ridge (Table 1). The Chefren mud volcano is located within the Menes
454 caldera in the Western Province ((Huguen et al., In review, this volume); Fig. 1A,E). The
455 center of this mud volcano hosts a large submarine lake of approximately 200m diameter
456 filled with fluidized mud and brines which were partially covered by mats of sulfide
457 oxidizers and their precipitates (Fig. 6A). The edges of the central lake were covered by
458 clear brines (Fig. 6B). In contrast, the center of the Napoli mud volcano had many
459 smaller sized brine pools of several meters to tens of meters, some of which were drained
460 (Fig. 4C). This area was previously investigated and further details of its geological,
461 geochemical and biological characteristics have been published elsewhere (Charlou et al.,
462 2003; Olu-Le Roy et al., 2004; Haese et al., 2006). We recovered 5 samples from the
463 slope (NL4PC1, NL18PC2(7) and PC4(6)) and center of Chefren (NL19PC1(5) and
464 PC3(8)), as well as 4 cores from the center of Napoli (NL1PC2, NL21PC5(1) and PC6(2),
465 NL22PC7(3)) (Table 1). All cores recovered from these seafloor areas were covered by

visible bacterial mats and their mineral precipitates, which varied considerably in color and composition.

At a mud cone on the NW flank of Chefren, colorful white and orange microbial mats were associated with brine seepage (Fig. 6D). These mats have been described in detail elsewhere (Omoregie et al., 2008). Briefly, the orange mats comprised sheaths of iron-oxidizing *Bacteria* as well as iron-oxide precipitates. The white mats comprised mainly sulfur filaments, produced by "*Candidatus* Arcobacter sulfidicus". Two cores (NL4PC1 and NL18PC4(6)) were retrieved from the sulfide-oxidizing mats and one core from iron-oxidizing mats (NL18PC2(7)) at the bottom of the north-western slope of Chefren (Tab. 1). Brine was observed flowing over the sulfide-oxidizing mats (Omoregie et al., 2008) and cores from these mats showed a highly reduced, blackish sediment horizon directly below the surface, followed by dark grey mud breccia (Fig. 7A). In contrast, the core from the iron-oxidizing mat (Fig. 7B) had a reduced layer in the middle of the core, which was surrounded by brownish sediment. The two cores from the center of Chefren were taken directly from the edge of a large brine lake in an area covered by clear brine (NL19PC1(5), PC3(8)). A thin line of bacterial mats formed directly between the interface of the brine and the seafloor (Fig. 6B). Both cores had reduced layers at the surface followed by dark brown sediment.

In the center of Napoli abundant patches of white bacterial mats (Fig. 6E) as well as extensive carbonate crusts were visible at the seafloor (Fig. 6F). These carbonate crusts were also frequently perforated with tube worms similar to the pockmark area of the Central NDSF. Two cores from thin sulfide-oxidizing mats (NL1PC2M and NL22PC3) and two cores from exposed blackish sediment between crusts (NL21PC1 and

2) were recovered from Napoli. All cores showed reduced sediment layers at the surface and dark grey sediment, interspersed with carbonate.

3.3.2 Sulfate reduction and anaerobic oxidation of methane

Methane concentrations in the bottom waters above the center of Chefren were relatively high (40 µM). In contrast those at Napoli were relatively low (20 nM) Mastalerz et al. unpublished data). The brines from both Chefren and Napoli (salinity of up to 153 and 268 ‰, respectively) contained high amounts of methane (up to 0.7 and 2.5 mM) and sulfide (up to 7.1 and 2.1 mM), but also sulfate (5-57 mM) (Huguen et al., In review, this volume). The sediments sampled from Chefren contained similar amounts of methane as found at the other seeps of the NDSF (0.2 - 2 mM). At Napoli, methane concentrations in the sediments were low (0.04 - 0.08 mM). The samples recovered from the Chefren and Napoli MV showed a wide range of SR and AOM rates (0.2 - 66.5 and 0.1 - 2.3 mmol cm^{-2} d^{-1}, 0 -10 cm). At both sites, SR exceeded AOM considerably, pointing to the presence of hydrocarbon sources other than methane (Fig. 7A-C and Table 3). The highest rates were generally located close to the surface, similar to the other cores investigated in this study. Sulfate concentrations remained very high throughout the cores, even close to the peaks of SR, possibly indicating advective transport by brine seepage (Fig. 7).

3.3.4 Microbial community structure

Similar to the 16S rRNA gene libraries of Amon and Isis, those from the slope of Chefren were dominated by sequences from the *Deltaproteobacteria* and ANME-2 or

512 ANME-3 (Table 5). Also, sequences of aerobic methanotrophs were abundant in samples
513 of mat and surface sediments. Total cell numbers in mat-covered sediments from the
514 slope of Chefren were slightly lower than those from the center of Amon and Isis (Table
515 4). ANME-2 and -3 cells only made up a small proportion of total archaeal cells,
516 indicating that other archaeal groups, such as MBGD may represent a significant biomass
517 in these sediment zones. In contrast, a relatively high proportion of the b*acterial* cells
518 were identified as sulfate reducers targeted by the DSS658 probe.

519 The cell numbers in surface sediments recovered from Napoli of around 2×10^{10}
520 cells $\times$ ml^{-1} were very high, but decreased within a few cm below the surface to numbers
521 similar to the other mud volcanoes in this study. The composition of Archaea at Napoli
522 was different from other cold seeps in the NDSF. ANME-1 cells appeared to be the
523 dominant ANME in the core from Napoli and ANME-2 were absent. Very few consortia
524 were detected in the Napoli sediments. *Bacteria* of the *Desulfosarcina*/*Desulfococcus*
525 cluster were abundant as free-living cells. This matched previous work conducted on
526 sediments and carbonates recovered from Napoli (Pancost et al., 2000; Aloisi et al., 2002;
527 Heijs, 2005). These studies detected highly ^{13}C-depleted biomarkers of *Archaea* and SRB,
528 as well as 16S rRNA gene sequences from Napoli sediments, which were representative
529 for ANME-1 and DSS groups.

530 Comparisons between the bacterial libraries of sediments underlying the sulfide-
531 and iron-oxidizing mats at Chefren indicated that they were significantly different (P
532 value < 1 %). Despite the proximity of the cores (<2 m distance), the difference in
533 microbial community structure was not surprising given the markedly different
534 geochemistry between these two mats, especially with regard to dissolved iron and

sulfide in the pore-waters (Omoregie et al., 2008).Comparisons of the archaeal and bacterial 16S rRNA gene libraries between the brine impacted mud volcano Chefren, to those of Amon and Isis indicated that they were significantly different (P value <1%). This suggests that the presence of brine may affect bacterial and archaeal community structure, but not necessarily their function, e.g. sulfate reduction. This phenomenon has already been observed in hypersaline photosynthetic communities (Clavero et al., 2000; Nubel et al., 2000).

4. Summary

Here, we have provided AOM and SR measurements from cold seeps in the Eastern Mediterranean. We show that the geology, chemistry and biology of these seep environments are considerably influenced by microbial processes as indicated in previous studies; hydrocarbon-driven sulfate reduction leads to the formation of anoxic microbial habitats, carbonate precipitates and bacterial mats, all of which provide habitats for associated fauna.

Only some of the investigated sediments showed a relatively tight coupling between AOM and sulfate reduction (e.g. North Alex, Amon), indicated that at most sites compounds other than methane were fueling sulfate reduction. At the active centres of the Amon, Isis, North Alex, Chefren and Napoli mud volcanoes SR and AOM rates of 1-10 mmol x m^{-2} x d^{-1} were measured. These rates are lower than at other known seep systems, such as Hydrate Ridge (NE Pacific) and the Bush Hill site (Gulf of Mexico) with AOM and SR rates of 50 - 100 mmol m^{-2} d^{-1} in sediments associated with bacterial mats (Treude et al., 2003; Joye et al., 2004). The range of SR and AOM rates of the E.

Mediterranean mud volcanoes matches seeps either limited by electron donor flux such as at mud volcanoes in the Gulf of Cadiz (Niemann et al., 2006a), or by electron acceptor depletion as at the Haakon Mosby mud volcano on the Norwegian margin (Niemann et al., 2006b). In this study, sites with less than 100µM methane in the surface sediments had very low AOM rates, hence methane availability may have been one factor in controlling the AOM rates. But even at sites with high availability of methane, rates were comparatively low. We did not reach the sulfate-methane transition zone in most of the cores and sulfate concentrations were always above 5 mM within the top 20 cm of sediment. The relatively low SR and AOM rates at the investigated sites matched the relatively low biomass of AOM consortia. An unknown factor other than energy supply must control the standing stock of these key microorganisms at the cold seeps of the Eastern Mediterranean, causing a low efficiency of the microbial filter eliminating the methane flux to the ocean. Accordingly, strong methane anomalies were observed in the water columns of all mud volcanoes investigated in this study.

To better understand the control of microbial activity, the sulfate and methane flux, further studies are needed to reveal the diversity and quantities of electron donors available to the microbial communities. Furthermore, due to the high heterogeneity and local variation in advective flow at the mud volcano and pockmark sites, spatial sampling needs to be improved, and in situ biogeochemical measurements are needed for quantitative rate assessments.

Acknowledgements

We would like to thank the crew and captain of RV L'Atalante, the NAUTILE crew as well as the NAUTINIL scientific party for their excellent support with work at sea. Also we thank Viola Beier, Imke Busse, Tomas Wilkop, Afua Asante-Poku and Abena Asante-Poku for help with analyses, Katrin Knittel and Alban Ramette for scientific advice, and Andrew Bisset for helpful comments on this manuscript. The work of E.O., H.N., and A.B. in the ESF EUROCORES EUROMARGIN project MEDIFLUX was financially supported by ESF, DFG and the Max Planck Society.

588 **References**

589 Aloisi, G. et al., 2002. CH4-consuming microorganisms and the formation of carbonate
590 crusts at cold seeps. Earth and Planetary Science Letters, 203(1): 195-203.
591 Aloisi, G. et al., 2000. Methane-related authigenic carbonates of eastern Mediterranean
592 Sea mud volcanoes and their possible relation to gas hydrate destabilisation. Earth
593 and Planetary Science Letters, 184(1): 321-338.
594 Bayon, G. et al., In review, this volume. In situ investigation of the Centre Nile margin:
595 Linking fluid seepage and continental-slope instabilities Marine Geology.
596 Bayon, G. et al., Submitted. In situ investigation of the Centre Nile margin: Linking fluid
597 seepage and continental-slope instabilities Marine Geology.
598 Boetius, A., Ferdelman, T. and Lochte, K., 2000a. Bacterial activity in sediments of the
599 deep Arabian Sea in relation to vertical flux. Deep Sea Res., 47: 2835-2875.
600 Boetius, A. and Lochte, K., 1996. Effect of organic enrichments on hydrolytic potentials
601 and growth of bacteria in deep-sea sediments. Mar. Ecol. Prog. Ser., 140: 239-250.
602 Boetius, A. et al., 2000b. A marine microbial consortium apparently mediating anaerobic
603 oxidation of methane. Nature, 407: 623-626.
604 Bouloubassi, I. et al., 2006. Archaeal and bacterial lipids in authigenic carbonate crusts
605 from eastern Mediterranean mud volcanoes. Organic Geochemistry, 37(4): 484-
606 500.
607 Camerlenghi, A., Cita, M.B., Hieke, W. and Ricchiuto, T., 1992. Geological Evidence for
608 Mud Diapirism on the Mediterranean Ridge Accretionary Complex. Earth and
609 Planetary Science Letters, 109(3-4): 493-504.

610 Charlou, J.L. et al., 2003. Evidence of methane venting and geochemistry of brines on
611 mud volcanoes of the eastern Mediterranean Sea. Deep-Sea Research Part I
612 Oceanographic Research Papers, 50(8): 941-958.
613 Clavero, E., Hernandez-Marine, M., Grimalt, J.O. and Garcia-Pichel, F., 2000. Salinity
614 tolerance of diatoms from thalassic hypersaline environments. Journal of
615 Phycology, 36(6): 1021-1034.
616 Coleman, D.F. and Ballard, R.D., 2001. A highly concentrated region of cold
617 hydrocarbon seeps in the southeastern Mediterranean Sea. Geo-Marine Letters,
618 21(3): 162-167.
619 Dolson, J.C., Boucher, P.J., Dodd, T. and Ismail, J., 2002. Petroleum potential of an
620 emerging giant gas province, Nile Delta and Mediterranean Sea off Egypt. Oil &
621 Gas Journal, 100(20): 32-37.
622 Dupré, S. et al., 2007. Seafloor geological studies above active gas chimneys off Egypt
623 (Central Nile Deep Sea Fan). Deep-Sea Research Part I: Oceanographic Research
624 Papers, 54(7): 1146-1172.
625 Fusi, N. and Kenyon, N.H., 1996. Distribution of mud diapirism and other geological
626 structures from long-range sidescan sonar (GLORIA) data, in the Eastern
627 Mediterranean Sea. Marine Geology, 132(1-4): 21-38.
628 Haese, R.R., Hensen, C. and de Lange, G.J., 2006. Pore water geochemistry of eastern
629 Mediterranean mud volcanoes: Implications for fluid transport and fluid origin.
630 Marine Geology, 225(1-4): 191-208.
631 Haese, R.R., Meile, C., Van Cappellen, P. and De Lange, G.J., 2003. Carbon
632 geochemistry of cold seeps: Methane fluxes and transformation in sediments from

633 Kazan mud volcano, eastern Mediterranean Sea. Earth and Planetary Science
634 Letters, 212(3-4): 361-375.
635 Heijs, S., 2005. Microbial communiteis at deep-sea mud volcanoes in the Eastern
636 Mediterranean Sea. PhD dissertation.
637 Heijs, S.K. et al., 2006. Microbial community structure in three deep-sea carbonate crusts.
638 Microbial Ecology, 52(3): 451-462.
639 Heijs, S.K., Damste, J.S.S. and Forney, L.J., 2005. Characterization of a deep-sea
640 microbial mat from an active cold seep at the Milano mud volcano in the Eastern
641 Mediterranean Sea. Fems Microbiology Ecology, 54(1): 47-56.
642 Hinrichs, K.-U. and Boetius, A., 2002. The anaerobic oxidation of methane: new insights
643 in microbial ecology and biogeochemistry. In: G. Wefer et al. (Editors), Ocean
644 Margin Systems. Springer-Verlag, Berlin, pp. 457-477.
645 Huguen, C. et al., In review, this volume. The Western Nile Margin Fluid seepages
646 features: “in situ” observations of the Menes caldera (NAUTINIL Expedition,
647 2003). Marine Geology.
648 Huguen, C. et al., 2004. Structural setting and tectonic control of mud volcanoes from the
649 Central Mediterranean Ridge (Eastern Mediterranean). Marine Geology, 209(1-4):
650 245-263.
651 Huguen, C., Mascle, J., Woodside, J., Zitter, T. and Foucher, J.P., 2005. Mud volcanoes
652 and mud domes of the Central Mediterranean Ridge: Near-bottom and in situ
653 observations. Deep-Sea Research Part I Oceanographic Research Papers, 52(10):
654 1911-1931.

655 Ishii, K., Mussmann, M., MacGregor, B.J. and Amann, R., 2004. An improved
656 fluorescence in situ hybridization protocol for the identification of bacteria and
657 archaea in marine sediments. FEMS Microbiology Ecology, 50(3): 203-213.
658 Iversen, N. and Blackburn, T.H., 1981. Seasonal rates of methane oxidation in anoxic
659 marine sediments. Applied and Environmental Microbiology, 41(6): 1295-1300.
660 Joye, S.B. et al., 2004. The anaerobic oxidation of methane and sulfate reduction in
661 sediments from Gulf of Mexico cold seeps. Chemical Geology, 205: 219-238.
662 Kallmeyer, J., Ferdelman, T.G., Weber, A., Fossing, H. and Jørgensen, B.B., 2004.
663 Evaluation of a cold chromium distillation procedure for recovering very small
664 amounts of radiolabeled sulfide related to sulfate reduction measurements. .
665 Limnology and Oceanography Methods, 2: 171-180.
666 Kane, M.D., Poulsen, L.K. and Stahl, D.A., 1993. Monitoring the enrichment and
667 isolation of sulfate-reducing bacteria by using oligonucleotide hybridization
668 probes designed from environmentally derived 16S rRNA sequences. Applied and
669 Environmental Microbiology, 59: 682-686.
670 Kniemeyer, O. et al., 2007. Anaerobic oxidation of short-chain hydrocarbons by marine
671 sulphate-reducing bacteria. Nature, 449(7164): 898-U10.
672 Knittel, K. et al., 2003. Activity, distribution, and diversity of sulfate reducers and other
673 bacteria in sediments above gas hydrate (Cascadia margin, Oregon).
674 Geomicrobiology Journal, 20(4): 269-294.
675 Knittel, K., Losekann, T., Boetius, A., Kort, R. and Amann, R., 2005. Diversity and
676 distribution of methanotrophic archaea at cold seeps. Applied and Environmental
677 Microbiology, 71(1): 467-479.

678 Lane, D.J. et al., 1985. Rapid-Determination of 16s Ribosomal-Rna Sequences for
679 Phylogenetic Analyses. Proceedings of the National Academy of Sciences of the
680 United States of America, 82(20): 6955-6959.
681 Levin, L.A., 2005. Ecology of cold seep sediments: Interactions of fauna with flow,
682 chemistry and microbes. Oceanography and Marine Biology - an Annual Review,
683 Vol. 43, 43: 1-46.
684 Loncke, L., Gaullier, V., Mascle, J., Vendeville, B. and Camera, L., 2006. The Nile deep-
685 sea fan: An example of interacting sedimentation, salt tectonics, and inherited
686 subsalt paleotopographic features. Marine and Petroleum Geology, 23(3): 297-
687 315.
688 Loncke, L., Mascle, J. and Fanil Scientific Parties, 2004. Mud volcanoes, gas chimneys,
689 pockmarks and mounds in the Nile deep-sea fan (Eastern Mediterranean):
690 geophysical evidences. Marine and Petroleum Geology, 21(6): 669-689.
691 Lösekann, T. et al., 2007. Diversity and Abundance of Aerobic and Anaerobic Methane
692 Oxidizers at the Haakon Mosby Mud Volcano, Barents Sea. Applied and
693 Environmental Microbiology. Applied and Environmental Microbiology, 73:
694 3348-3362.
695 Ludwig, W. et al., 2004. ARB: a software environment for sequence data. Nucleic Acids
696 Research, 32(4): 1363-1371.
697 Luff, R. and Wallmann, K., 2003. Fluid flow, methane fluxes, carbonate precipitation and
698 biogeochemical turnover in gas hydrate-bearing sediments at Hydrate Ridge,
699 Cascadia Margin: numerical modeling and mass balances. Geochimica et
700 Cosmochimica Acta, 67(18): 3403-3421.

701 Mascle, J., Loncke, L. and Camera, L., 2005. Geophysical evidences of fluid seepages
702 and mud volcanoes on the Egyptian continental margin (Eastern Mediterranean).
703 Bollettino Della Societa Geologica Italiana: 127-134.
704 Mascle, J. et al., 2006. Morphostructure of the Egyptian continental margin: Insights
705 from swath bathymetry surveys. Marine Geophysical Researches, 27(1): 49-59.
706 Mascle, J. et al., 2001. The Nile deep sea fan: preliminary results from a swath
707 bathymetry survey. Marine and Petroleum Geology, 18(4): 471-477.
708 Massana, R., Murray, A.E., Preston, C.M. and DeLong, E.F., 1997. Vertical distribution
709 and phylogenetic characterization of marine planktonic Archaea in the Santa
710 Barbara Channel. Applied and Environmental Microbiology, 63(1): 50-56.
711 Michaelis, W. et al., 2002. Microbial reefs in the Black Sea fueled by anaerobic oxidation
712 of methane. Science, 297: 1013-1015.
713 Mills, H.J., Martinez, R.J., Story, S. and Sobecky, P.A., 2005. Characterization of
714 microbial community structure in Gulf of Mexico gas hydrates: Comparative
715 analysis of DNA- and RNA-derived clone libraries. Applied and Environmental
716 Microbiology, 71(6): 3235-3247.
717 Muyzer, G., Teske, A., Wirsen, C.O. and Jannasch, H.W., 1995. Phylogenetic-
718 Relationships of Thiomicrospira Species and Their Identification in Deep-Sea
719 Hydrothermal Vent Samples by Denaturing Gradient Gel-Electrophoresis of 16s
720 Rdna Fragments. Archives of Microbiology, 164(3): 165-172.
721 Niemann, H. et al., 2006a. Microbial methane turnover at mud volcanoes of the Gulf of
722 Cadiz. Geochimica et Cosmochimica Acta, 70(21): 5336.

723 Niemann, H. et al., 2006b. Novel microbial communities of the Haakon Mosby mud
724 volcano and their role as a methane sink. Nature, 443(7113): 854.
725 Nubel, U., Garcia-Pichel, F., Clavero, E. and Muyzer, G., 2000. Matching molecular
726 diversity and ecophysiology of benthic cyanobacteria and diatoms in communities
727 along a salinity gradient. Environ Microbiol, 2(2): 217-226.
728 Olu-Le Roy, K. et al., 2004. Cold seep communities in the deep eastern Mediterranean
729 Sea: composition, symbiosis and spatial distribution on mud volcanoes. Deep-Sea
730 Research Part I: Oceanographic Research Papers, 51(12): 1915-1936.
731 Omoregie, E.O. et al., 2008. Biogeochemistry and community composition of iron- and
732 sulfur-precipitating microbial mats at the Chefren mud volcano Applied and
733 Environmental Microbiology, 74(10): 3198-3215.
734 Orphan, V.J., House, C.H., Hinrichs, K.-U., McKeegan, K.D. and De Long, E.F., 2001.
735 Methane-consuming Archaea revealed by directly coupled isotopic and
736 phylogenetic analysis. Science, 293: 484-487.
737 Pancost, R.D. et al., 2000. Biomarker evidence for widespread anaerobic methane
738 oxidation in Mediterranean sediments by a consortium of methanogenic archaea
739 and bacteria. Applied and Environmental Microbiology, 66(3): 1126-1132.
740 Pernthaler, A. et al., 2008. Diverse syntrophic partnerships from-deep-sea methane vents
741 revealed by direct cell capture and metagenomics. Proceedings of the National
742 Academy of Sciences of the United States of America, 105(19): 7052-7057.
743 Pernthaler, A., Pernthaler, J. and Amann, R., 2002. Fluorescence in situ hybridization and
744 catalyzed reporter deposition (CARD) for the identification of marine Bacteria.
745 Applied and Envrionmental Microbiol(68): 3094-3101.

746 Reeburgh, W.S., 2007. Oceanic methane biogeochemistry. Chemical Reviews, 107(2):
747 486-513.
748 Ritger, S., Carson, B. and Suess, E., 1987. Methane-Derived Authigenic Carbonates
749 Formed by Subduction Induced Pore-Water Expulsion Along the Oregon
750 Washington Margin. Geological Society of America Bulletin, 98(2): 147-156.
751 Sahling, H., Rickert, D., Lee, R.W., Linke, P. and Suess, E., 2002. Macrofaunal
752 community structure and sulfide flux at gas hydrate deposits from the Cascadia
753 convergent margin, NE Pacific. Marine Ecology Progress Series, 231: 121-138.
754 Schloss, P.D., Larget, B.R. and Handelsman, J., 2004. Integration of microbial ecology
755 and statistics: a test to compare gene libraries. Applied and Environmental
756 Microbiology, 70(9): 5485-5492.
757 Sibuet, M. and Olu-Le Roy, K., 2002. Cold Seep Communities on Continental Margins:
758 Structure and Quantitative Distribution Relative to Geological and Fluid Venting
759 Patterns, Ocean Margin System. Springer Verlag, pp. 235-251.
760 Sibuet, M. and Olu, K., 1998. Biogeography, biodiversity and fluid dependence of deep-
761 sea cold-seep communities at active and passive margins. Deep-Sea Research Part
762 II: Topical Studies in Oceanography, 45(1-3): 517-567.
763 Snaidr, J., Amann, R., Huber, I., Ludwig, W. and Schleifer, K.H., 1997. Phylogenetic
764 analysis and in situ identification of bacteria in activated sludge. Applied and
765 Environmental Microbiology, 63(7): 2884-2896.
766 Tina Lösekann et al., 2007. Diversity and abundance of aerobic and anaerobic methane
767 oxidizers at the Haakon Mosby Mud Volcano, Barents Sea Applied and
768 Environmental Microbiology, 73: 3348-3362.

769 Treude, T., Boetius, A., Knittel, K., Wallmann, K. and Jørgensen, B.B., 2003. Anaerobic
770 oxidation of methane above gas hydrates at Hydrate Ridge, NE Pacific Ocean.
771 Marine Ecology Progress Series, 264: 1-14.
772 Wallmann, K. et al., 1997. Quantifying fluid flow, solute mixing, and biogeochemical
773 turnover at cold vents of the eastern Aleutian subduction zone. Geochim.
774 Cosmochim. Acta, 61(24): 5209-5219.
775 Widdel, F., Musat, F., Knittel, K. and Galushko, A., 2006/2007. Anaerobic degradation
776 of hydrocarbons with sulphate as electron acceptor. In: L. Barton, L. and W.A.
777 Hamilton (Editors), Sulphate-Reducing Bacteria: Environmental and Engineered
778 Systems. Cambridge University Press.
779 Widdel, F. and Rabus, R., 2001. Anaerobic biodegradation of saturated and aromatic
780 hydrocarbons. Current Opinion in Biotechnology, 12(3): 259-276.
781 Woodside, J.M., Ivanov, M.K., Limonov, A.F. and Shipboard Scientist of the, A.E., 1998.
782 Shallow gas and gas hydrates in the Anaximander Mountains region, eastern
783 Mediterranean Sea. Geological Society, London, Special Publications, 137(1):
784 177-193.
785 Zitter, T.A.C., Huguen, C. and Woodside, J.M., 2005. Geology of mud volcanoes in the
786 eastern Mediterranean from combined sidescan sonar and submersible surveys.
787 Deep-Sea Research Part I: Oceanographic Research Papers, 52(3): 457-475.
788
789

790 **Table 1.** Sediment cores, and analysis conducted within this study. Latitude and longitude are given in degrees and decimal minutes.

Dive	Location[a]	Site	Latitude	Longitude	Depth (m)	Core ID	SO_4^{2-}	CH_4	SR	AOM	16S	FISH	Dive observation
11	E	Amon, SE center	32° 22.1444	31° 42.6481	1121	NL11PC1	x	x	x	x	-	-	sulfide oxidizing mat
12	E	Amon, SW center	32° 22.1418	31° 42.5926	1120	NL12PC2	x	x	x	x	x	x	sulfide oxidizing mat
8	E	Isis, center	32° 21.6619	31° 23.3714	992	NL8PC1(4)	-	x	x	x	-	-	sulfide oxidizing mat
8	E	Isis, center	32° 21.6678	31° 23.3572	992	NL8PC3(1)	x	x	x	x	-	-	gas saturated grayish sediment
13	E	Isis, NW center	32° 21.6779	31° 23.3370	991	NL13PC4(7)	x	x	x	x	x	x	sulfide oxidizing mat
6	C	Pockmarks, middle slope	32° 38.1418	29° 56.1236	2114	NL6PC1	x	x	x	x	-	-	within a pockmark
7	C	Pockmarks, middle slope	32° 31.6062	30° 20.6553	1691	NL7PC1	-	x	x	x	-	-	away from pockmarks and carbonate
14	C	Pockmarks, lower slope	32° 38.4402	29° 54.9764	2127	NL14PC2	-	x	x	x	-	x	close to carbonate
15	C	North Alex, E center	31° 58.1897	30° 08.2229	507	NL15BC1	x	x	x	x	x	-	grey sediment without mats
4	W	Chefren, NW slope	32°.06 7373	28° 10.3497	3023	NL4PC1	-	x	x	x	-	-	sulfide oxidizing mat
18	W	Chefren, NW slope	32° 06.7406	28° 10.3487	3024	NL18PC2(7)	x	x	x	x	x	x	iron oxidizing mat
18	W	Chefren, NW slope	32° 06.7397	28° 10.3510	3022	NL18PC4(6)	x	x	x	x	x	x	sulfide oxidizing mat
19	W	Chefren, S center	32° 06.4872	28° 10.6767	2968	NL19PC1(5)	x	x	x	x	-	-	the edge of a brine lake
19	W	Chefren, S center	33° 06.4872	28° 10.6774	2968	NL19PC3(8)	x	-	x	x	-	x	the edge of a brine lake
1	MR	Napoli, center	33° 43.4759	24° 41.0472	1939	NL1PC2	x	x	x	x	-	x	sulfide oxidizing mat
21	MR	Napoli, NW center	33° 43.6553	24° 40.8541	1946	NL21PC5(1)			x	x	-	-	sulfide oxidizing mat
21	MR	Napoli, NW center	34° 43.6553	24° 40.8541	1946	NL21PC6(2)	x	x	x	x	-	-	sulfide oxidizing mat
22	MR	Napoli, S center	33° 43.3569	24° 41.0522	1940	NL22PC7(3)	x	x	x	x	-	-	sulfide oxidizing mat

791

792 a. Location within the Eastern (E), Central (C) and Western (W) Nile Deep-Sea fan, as well as the Mediterranean Ridge (MR).

Table 2. Oligonucleotide probes and hybridization conditions used in this study. EUB-I, II, III were mixed into a single solution.

Probe	Target Group	Sequence (5' to 3')	Type	%Formamid	°C Hybrid/Wash	Reference
ARCH915	Most Archaea	GTGCTCCCCCGCCAATTCCT	CARD	35	46/48	Amann et al. 1990
ANME-1-350	ANME-1	AGTTTTCGCGCCTGATGC	CARD	40	46/48	Boetius *et al.* 2000
ANME-2-538	ANME-2	GGCTACCACTCGGGCCGC	FISH	50	46/48	Treude *et al.* 2005
ANME-3-1249	ANME-3	TCGGAGTAGGGACCCATT	CARD	20	46/48	Lösekann *et al.* 2007
EUB I	Most bacteria	GCTGCCTCCCGTAGGAGT	CARD	35	46/48	Amann et al. 1990
EUB II	*Planctomycetales*	GCAGCCACCCGTAGGTGT	CARD	35	46/48	Daims *et al.* 1999
EUB III	*Verrucomicrobiales*	GCTGCCACCCGTAGGTGT	CARD	35	46/48	Daims *et al.* 1999
Non338	negative hybridization probe	ACTCCTACGGGAGGCAGC	CARD/FISH	variable	46/48	Wallner *et al.* 1993
DSS658	*Desulfosarcina-Desulfococcus*	TCCACTTCCCTCTCCCAT	CARD	50	46/48	Manz *et al.* 1998
660	*Desulfobulbus*	GAATTCCACTTTCCCCTCTG	CARD	60	46/48	Devereux *et al.* 1992
Mγ705	Type I Methanotrophs	CTGGTGTTCCTTCAGATC	FISH	20	46/48	Gulledge *et al.* 1992

Table 3. Depth integrated sulfate reduction (SR) and anaerobic oxidation of methane (AOM) rates in different sediment horizons (mmol × m^{-2} × d^{-1}). "<" indicates less than 0.01 mmol × m^{-2} × d^{-1}.

Location	Core	SR(0-4)	AOM(0-4)	SR/AOM	SR (4-10)	AOM(4-10)	SR/AOM	SR(0-10)	AOM(0-10)	SR/AOM	SR (10-)	AOM(10-)	SR/AOM	core depth
Amon	NL11PC1	2.0	0.1	**15**	8.5	3.0	**3**	10.5	3.1	**3**	10.7	0.8	**14**	(23cm)
Amon	NL12PC2	9.9	2.2	**5**	6.8	3.7	**2**	16.7	5.8	**3**	2.8	0.8	**3**	(15cm)
Isis	NL8PC1(4)	3.2	0.2	**14**	0.7	0.1	**6**	3.8	0.3	**12**	-	-	-	
Isis	NL8PC3(1)	3.3	0.2	**14**	5.3	0.1	**57**	8.6	0.3	**26**	-	-	-	
Isis	NL13PC4(7)	24.8	1.5	**17**	19.1	2.1	**9**	44.0	3.6	**12**	-	-	-	
Pockmarks	NL6PC1	0.1	<	-	<	<	-	0.1	<	-	-	-	-	
Pockmarks	NL7PC1	<	<	-	<	<	-	<	<	-	-	-	-	
Pockmarks	NL14PC2	0.1	0.1	**1**	0.1	<	-	0.1	0.1	**2**	2.8	<	-	(21cm)
North Alex	NL15BC1	1.2	0.9	**1**	2.8	2.5	**1**	4.0	3.5	**1**	-	-	-	
Chefren	NL4PC1	42.7	0.6	**72**	23.9	0.3	**79**	66.5	**0.9**	**75**	2.1	0.2	**10**	(25cm)
Chefren	NL18PC4(6)	4.1	0.1	**72**	0.3	0.1	**3**	4.4	0.2	**28**	-	-	-	
Chefren	NL18PC2(7)	0.8	0.2	**4**	4.6	0.3	**16**	5.3	0.5	**11**	0.6	0.1	**6**	(15cm)
Chefren	NL19PC3(8)	0.2	0.2	**1**	<	0.1	-	0.2	0.3	**1**	-	-	-	
Chefren	NL19PC1(5)	0.5	1.2	-	0.1	1.1	-	0.7	2.3	-	-	-	-	
Napoli	NL1PC2	8.7	<	-	0.1	<	-	8.8	<	-	-	-	-	
Napoli	NL21PC6(2)	2.0	<	-	0.1	<	-	2.1	<	-	-	-	-	
Napoli	NL21PC5(1)	4.4	0.1	**70**	3.6	<	-	8.0	0.1	**87**	27.1	<	-	(13cm)
Napoli	NL22PC7(3)	0.6	<	-	3.6	<	-	4.2	<	-	-	-	-	

Table 4. Cell numbers as well as FISH counts for Archaea and *Bacteria*. ANME-3-1249 and 660 targeted cells were less than 1 % of total cell numbers. Numbers are per ml of sediment.

			ARC915			ANME-1			ANME-2			EUBI-III			DSS658			Mγ705		
	Depth	Total Cells 1x109	Free Cells $1x10^9$	Cells in Agg$1x10^9$	Percent Total	Free Cells $1x10^9$	Cells in Agg$1x10^9$	Percent Total	Free Cells $1x10^9$	Cells in Agg$1x10^9$	Percent Total	Free Cells $1x10^9$	Cells in Agg$1x10^9$	Percent Total	Free Cells $1x10^9$	Cells in Agg$1x10^9$	Percent Total	Free Cells $1x10^9$	Cells in Agg$1x10^9$	Percent Total
Amon	**0-2cm**	8.03	0.05	3.38	43	<	<	<	<	1.79	22	0.99	3.38	54	0.05	3.98	50	<	<	<
NL12PC1	**2-4cm**	7.40	0.06	3.13	43	<	<	<	<	0.76	10	0.95	3.13	55	0.08	2.27	32	<	<	<
	10-12cm	0.30	0.01	0.00	5	<	<	<	<	<	<	0.11	0.00	38	0.01	nd	2	<	<	<
Isis	**0-2cm**	4.87	0.26	1.33	33	<	<	<	<	0.54	11	1.65	1.33	61	0.09	0.06	3	<	<	<
NL13PC4(7)	**2-4cm**	7.44	0.05	3.02	41	<	<	<	<	2.56	34	0.73	3.02	50	0.21	0.01	3	<	<	<
	10-12cm	3.96	0.11	1.44	39	<	<	<	<	-	-	0.86	1.44	58	0.07	0.01	2	<	<	<
PockM	**0-2cm**	0.67	0.11	<	17	<	<	<	<	<	<	0.32	<	47	<	<		<	<	<
NL14PC2	**2-4cm**	0.88	0.02	<	2	<	<	<	<	<	<	0.22	<	24	<	<		0.01	<	2
	10-12cm	0.41	0.01	<	3	<	<	<	<	<	<	0.08	<	19	<	<			<	<
North A.	**0-2cm**	3.52	0.11	0.50	17	0.02	<	0	<	0.46	13	2.08	0.50	73	0.25	0.02	7	<	<	<
NL15BC1	**2-4cm**	3.62	0.04	0.41	13	0.01	<	0	<	<	<	2.44	0.41	79	0.30	0.00	8	<	<	<
	10-12cm	2.70	0.09	0.55	24	0.03	<	1	<	0.18	7	0.16	0.55	27	0.06	0.00	3	<	<	<
Chefren	**0-2cm**	0.90	0.06	<	7	<	<	<	<	<	<	0.47	<	52	0.21	<	23	<	<	<
NL18PC4(6)	**2-4cm**	2.10	0.07	0.59	32	<	<	<	<	0.38	18	0.49	0.59	51	0.16	0.29	22	<	<	<
	10-12cm	0.42	0.07	<	17	<	<	<	<	<	<	0.13	<	30	<	<	<	<	<	<
Chefren	**0-2cm**	1.28	0.02	0.07	7	<	<	<	<	0.10	8	0.77	z 0.07	66	0.13	0.07	16	0.03	<	2
NL18PC2(7)	**2-4cm**	4.76	0.27	0.84	23	<	<	<	<	0.96	20	1.09	0.84	41	0.09	1.92	42	<	<	<
	10-12cm	4.59	0.34	<	7	<	<	<	<	<	<	0.16	<	3	0.13	<	3	<	<	<
Napoli	**0-2 cm**	20.45	3.27	3.12	31	1.04	<	5	<	<	<	5.96	3.12	44	2.35	<	11	0.06	<	1
NL1PC2	**2-4 cm**	1.80	0.32	<	18	0.16	<	9	<	<	<	0.76	<	42	0.13	<	7	0.00	<	1
	10-12 cm	1.99	0.66	<	33	0.43	<	22	<	<	<	0.54	<	27	<	<	0	<	<	<

804 **Table 5.** Breakdown of 16S rRNA gene sequences, in percentages obtained from selected

805 cores in this study. The first 4 cm of sediment was used to construct each library.

806

Phylogenetic group	Amon (NL12PC1)	Isis (NL12PC1)	Chefren (NL18PC4(6))	Chefren (NL18PC2(7))
Total number of *Bacterial* clones	**79**	**64**	**83**	**88**
% *Alphaproteobacteria*	**1**	**5**	**0**	**1**
% *Gammaproteobacteria*	**25**	**20**	**8**	**34**
% Type I methanothrophs	8	5	2	7
% *Deltaproteobacteria*	**58**	**36**	**42**	**31**
% SRB-1 *Desulfosarcina\Desulfococcus*	25	19	14	9
% SRB-2	0	0	1	0
% SRB-3 *Desulfobulbus*	1	0	0	1
% SRB-4	5	2	1	1
% *Epsilonproteobacteria*	**1**	**6**	**0**	**7**
% Other *Bacteria*	**13**	**33**	**42**	**22**
% Unidentified *Bacteria*	**1**	**0**	**7**	**6**
Total number of *Archaeal* clones	**68**	**71**	**71**	**66**
% *Euryarcheaota*	**100**	**97**	**94**	**98**
% Methanococcoides	3	1	0	0
% ANME-undesignated	3	1	0	3
% ANME-2A	51	31	18	52
% ANME-2C	12	8	1	3
% ANME-3	0	0	55	0
% MBG-D	15	51	15	36
% unidentified *Euryarcheaota*	16	4	6	5
% *Crenarcheaota*	**0**	**3**	**4**	**2**
% MBG-B	0	1	4	2
% MBG-1	0	1	0	0

807

Figure legends

Figure 1. (A) Bathymetric map of the Eastern Mediterranean. Small and large rectangles are the Olimpi mud volcano field and the Nile Deep Sea Fan, respectively. Numbers indicate the locations of the Napoli (1), Chefren (2), North Alex (5), Isis (6), and Amon (7) mud volcanoes as well as the pockmark region in the middle (3) and lower slope (4). (B) 3D-Bathymetric map of Amon and Isis using an EM 12 dual system. After (Dupré et al., 2007) (C) 3D-Bathymetric map of North Alex using an EM 12 dual system. (D) 3D-Bathymetric map of the pockmarks region using an EM 12 dual system. After (Mascle et al., 2006) (E) 3D-Bathymetric map of the Menes Caldera using an EM 12 dual system. (F) 3D-Bathymetric map of Napoli using an EM 120 dual system. Depth scale bar not shown, however, the summit of Napoli is about 1950 meters. Data collected in 2004 by the Simed survey on board the B.O. “Beautemps-Beaupré”. Numbers and lines in B,D,E indicate cruise tracks and dive numbers.

Figure 2. Seafloor images taken by the submersible Nautile. (A) Troughs at the center of Amon covered with sulfide oxidizing mats. (B) Troughs at the center of Isis covered with sulfide-oxidizing mats. (C) Flat seabed at Isis with sulfide-oxidizing mats (NL8PC1(4), NL13PC4(7)) and grey patches (NL8PC3(1)). (D) Carbonate crusts at the outer rim of Amon.

Figure 3. Rates of sulfate reduction and anaerobic oxidation of methane, and profiles of sulfate and methane concentrations from selected cores. Lines with triangles, squares and

831 circles are replicate rate measurements, whereas solid lines are sulfate and methane
832 measurements. Core descriptions presented on the right next to geochemical gradients.
833 Pictograms used for core descriptions are below. (A) Core from sulfide oxidizing mat of
834 Amon (NL12PC1). (B) Core from sulfide oxidizing mat of Isis (NL13PC4(7).
835
836 Figure 4. Seafloor images taken by the submersible Nautile. (A) Flat seabed of North
837 Alex (NL15BC) exhibiting gas ebullition. (B) Edge of a pockmark from middle slope
838 (Dive NL7). (C) Carbonate pavement of the lower slope (NL14PC2). (D) Close up of
839 siboglinid worms and shell debris from a carbonate crust.
840
841 Figure 5. Rates of sulfate reduction and anaerobic oxidation of methane, and profiles of
842 sulfate and methane concentrations from selected cores. Lines with triangles, squares and
843 circles are replicate rate measurements, whereas solid lines are sulfate and methane
844 measurements. For legend see Figure 3. (A) Gas saturated sediment from North Alex
845 (NL15BC1). (B) Next to a carbonate crust (NL14PC1). Pictograms used for core
846 descriptions are below are provided in figure 3
847
848 Figure 6. Seafloor images taken by the submersible Nautile. (A) Brine pool at Chefren
849 covered with sulfide-oxidizing mats. (B) Sediment (upper left) and brine transition,
850 bisected by sulfide-oxidizing mats at Chefren (NL19PC1(5) and PC3(8)). (C) Brine lake
851 at Napoli. (D) Sulfide and iron oxidizing mats at Chefren (NL4PC1, NL18PC2(7),
852 PC4(6)). (E) Sulfide-oxidizing mats and reduced sediment at Napoli (NL1PC2,
853 NL21PC5(1), PC6(2) and NL22PC7(3)). (F) Carbonate crusts at Napoli.

Figure 7. Rates of sulfate reduction and anaerobic oxidation of methane, and profiles of sulfate and methane concentrations from selected cores. Lines with triangles, squares and circles are replicate rate measurements, whereas solid lines are sulfate and methane measurements. For legend see Figure 3. (A) Sulfide-oxidizing mat from Chefren (NL18PC4(6)). (B) Iron-oxidizing mat from Chefren (NL18PC2(7)). (C) Sulfide-oxidizing mat from Napoli (NL1PC2). Pictograms used for core descriptions are provided in figure 3.

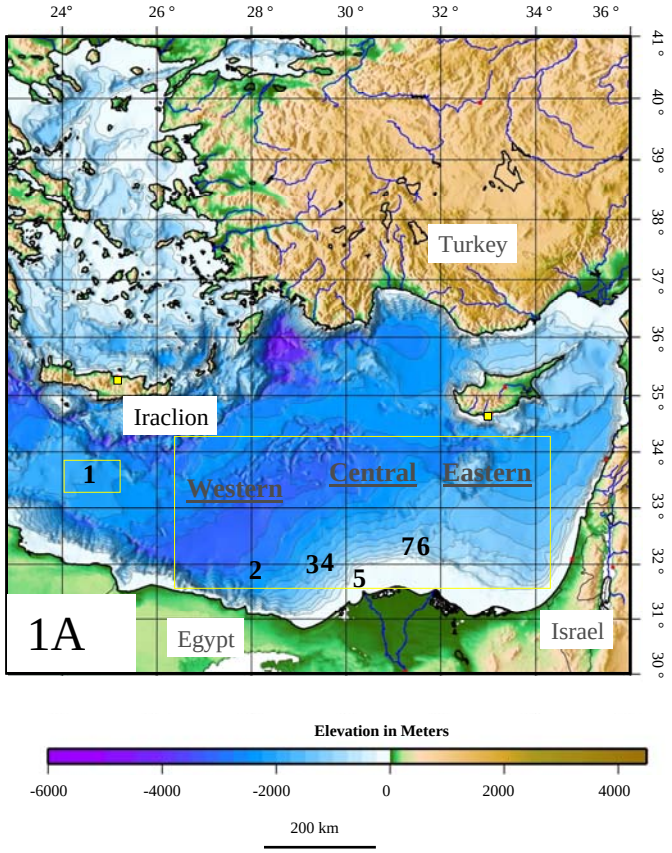
24°
26 °
28 °
30 °
32 °
34 °
36 °
41 °
40 °
39 °
38 °
37 °
36 °
35 °
34 °
33 °
32 °
31 °
30 °
Turkey
Iraclion
1
Western
Central
Eastern
2
34
5
76
1A
Egypt
Israel
Elevation in Meters
-6000
-4000
-2000
0
2000
4000
200 km

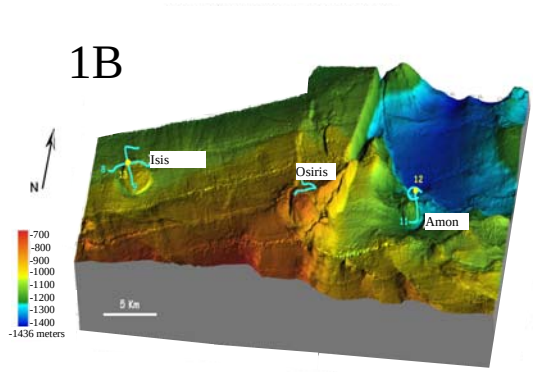
1B
Isis
Osiris
Amon
-700
-800
-900
-1000
-1100
-1200
-1300
-1400
-1436 meters
5 Km

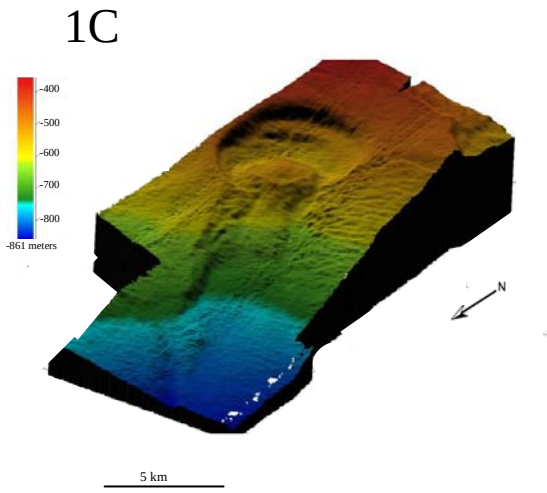
1C
-400
-500
-600
-700
-800
-861 meters
5 km

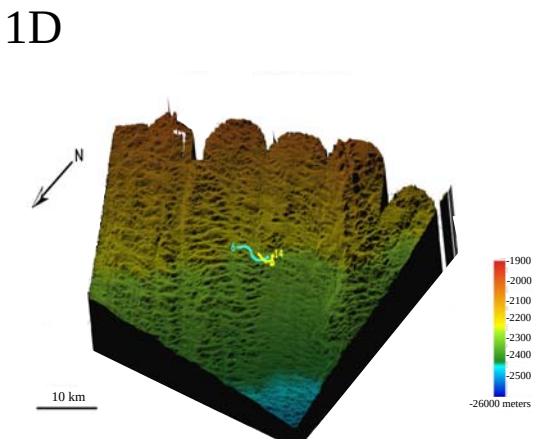
1D
N
10 km
-1900
-2000
-2100
-2200
-2300
-2400
-2500
-26000 meters

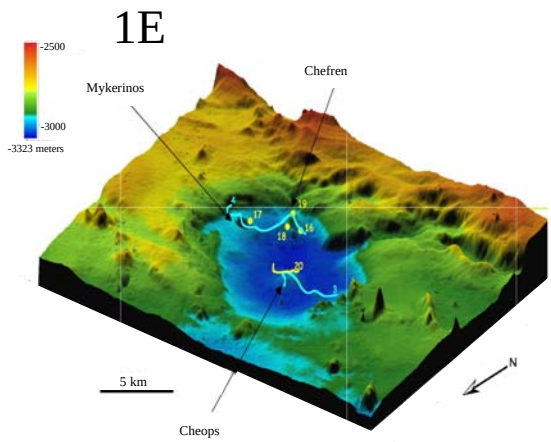
1E
-2500
-3000
-3323 meters
Mykerinos
Chefren
5 km
Cheops
N

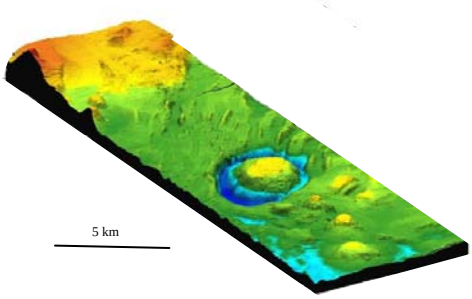
1F
5 km

Figure 1

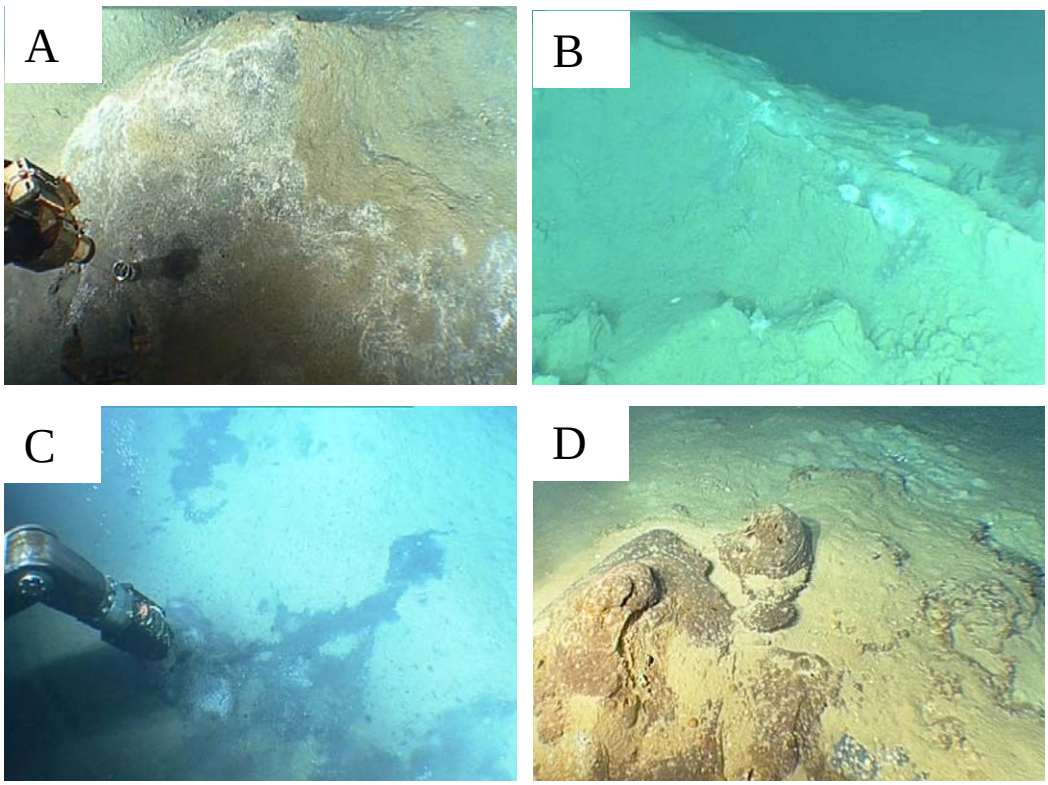

Figure 2

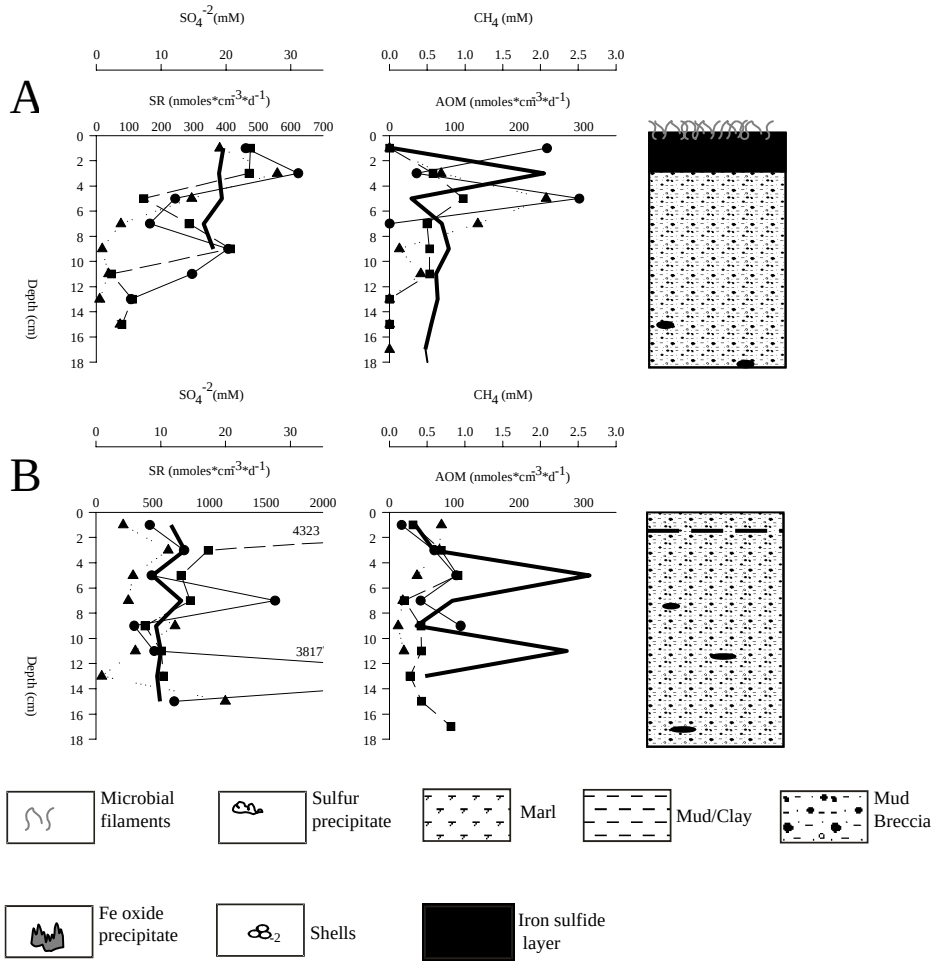
A
B
SO_4^{-2}(mM)
CH_4 (mM)
SR (nmoles*cm^{-3}*d^{-1})
AOM (nmoles*cm^{-3}*d^{-1})
Depth (cm)
4323
3817
Microbial filaments
Sulfur precipitate
Marl
Mud/Clay
Mud Breccia
Fe oxide precipitate
Shells
Iron sulfide layer

Figure 3

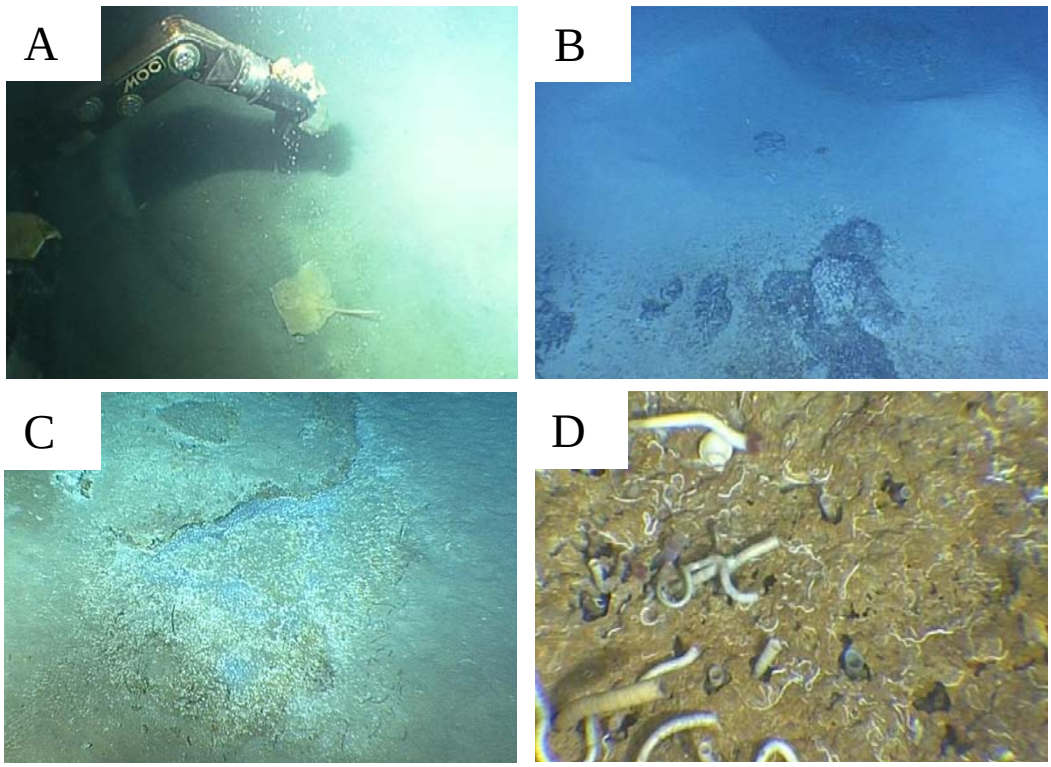

Figure 4

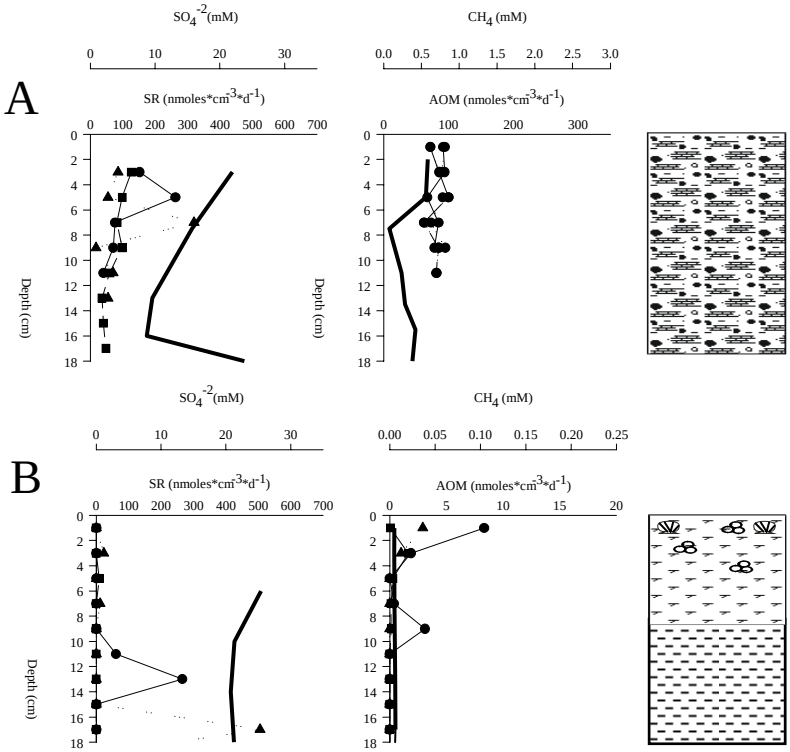
A
SO_4^{-2}(mM)
0 10 20 30
CH_4 (mM)
0.0 0.5 1.0 1.5 2.0 2.5 3.0
SR (nmoles*cm^{-3}*d^{-1})
0 100 200 300 400 500 600 700
AOM (nmoles*cm^{-3}*d^{-1})
0 100 200 300
Depth (cm)
0 2 4 6 8 10 12 14 16 18
B
SO_4^{-2}(mM)
0 10 20 30
CH_4 (mM)
0.00 0.05 0.10 0.15 0.20 0.25
SR (nmoles*cm^{-3}*d^{-1})
0 100 200 300 400 500 600 700
AOM (nmoles*cm^{-3}*d^{-1})
0 5 10 15 20
Depth (cm)
0 2 4 6 8 10 12 14 16 18

Figure 5

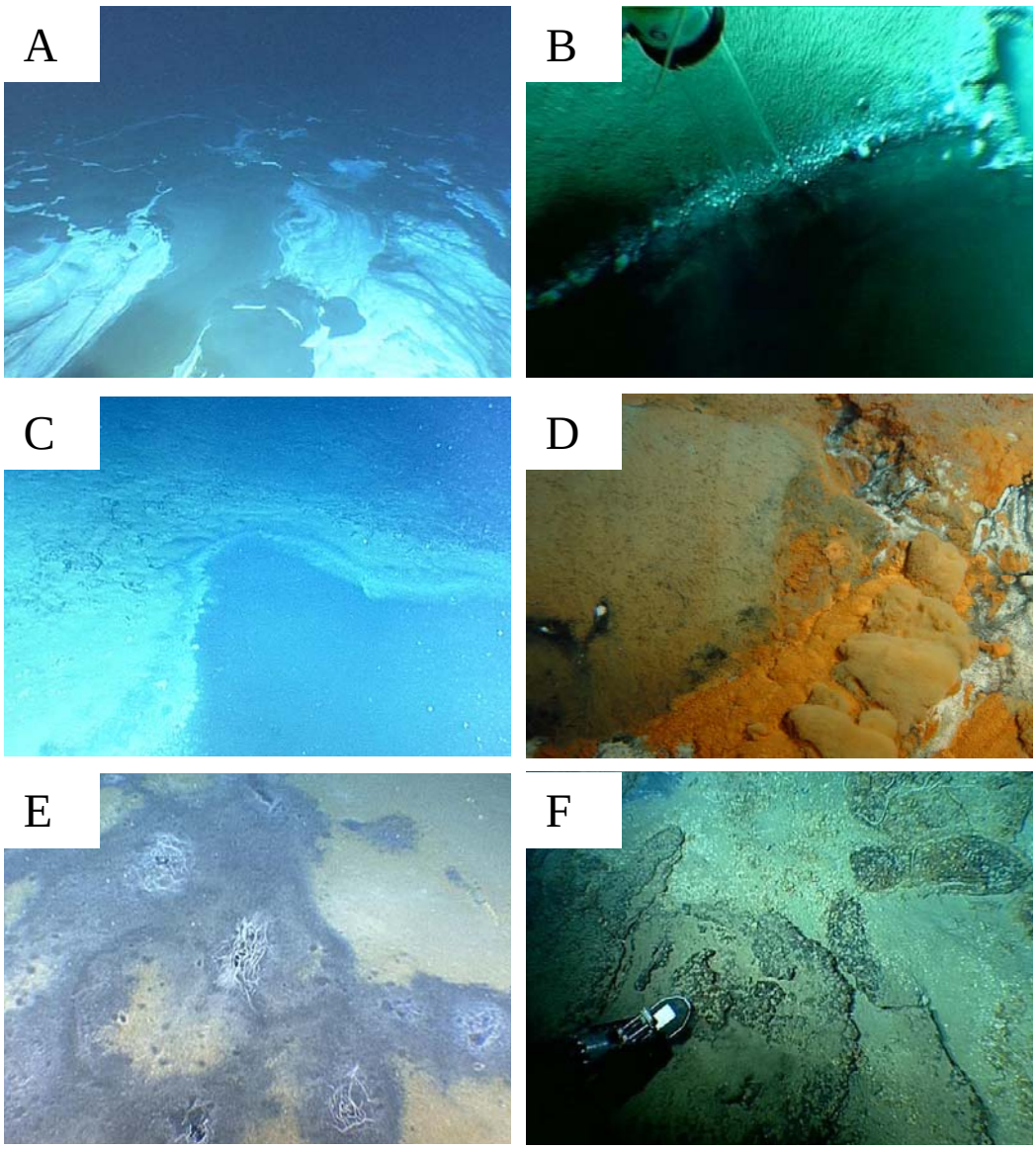

Figure 6

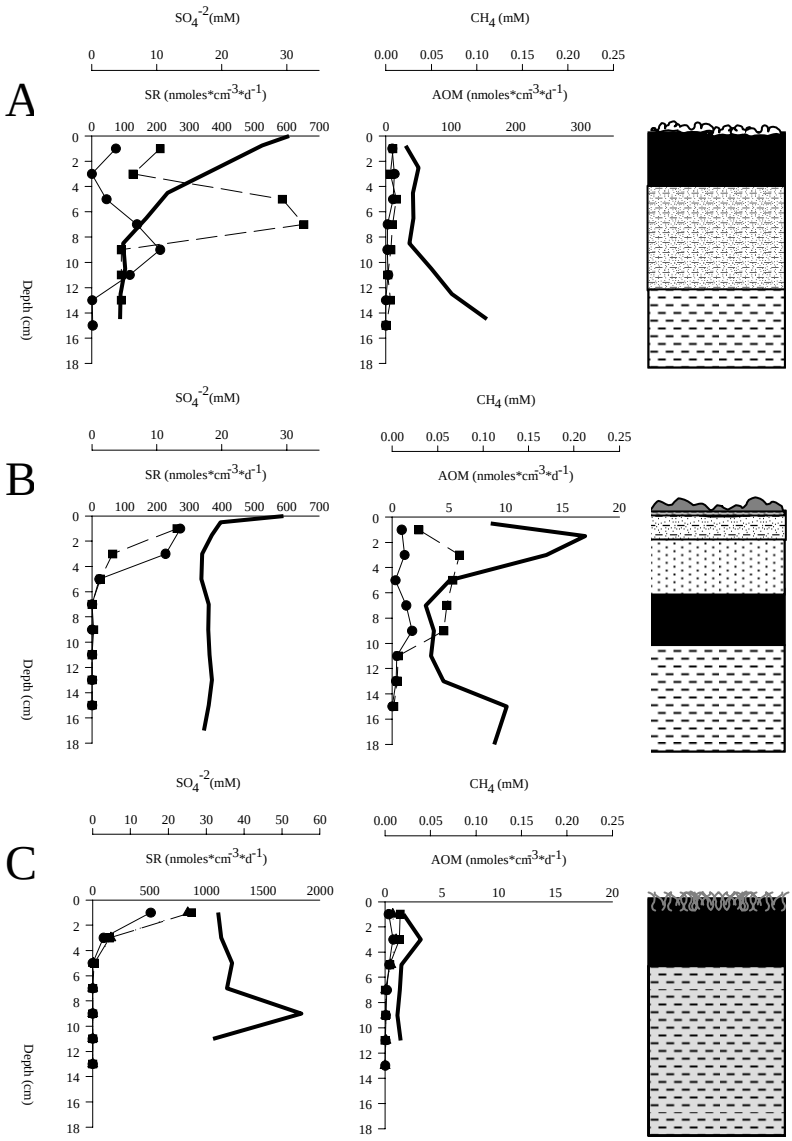

Figure 7